Nanoscale Structures and Modulations on Solid Surfaces Probed by X-ray Absorption Fine Structure

H. Oyanagi

Electrotechnical Laboratory
1-1-4 Umezono, Tsukuba, Ibaraki 305, Japan

(Received: Jan. 31, 1997 Accepted: Feb. 28, 1997)

Abstract

The recent developments in fluorescence-detected X-ray absorption fine structure (XAFS) using synchrotron radiation are briefly reviewed and results of applications to nanoscale structures are reported. For $YBa_2Cu_3O_{7-\delta}$ (1000Å), an anomaly in the mean-square relative displacement for the in-plane Cu-O bonds is observed at higher temperature than T_c (T^*~$1.5T_c$) which coincides the anomalies originating from the opening of a spin-gap. This suggests that the in-plane lattice anomaly is caused by a spin-phonon interacion as a short-range order of spin singlet is formed. *In-situ* monitoring of the local structure in amorphous selenium under illumination at low temperature shows the bond alternation associated with a photoexcitation. This suggests that the dominant process of photoexcitation of lone pair electrons is the formation of neutral three-fold coordinated defect pairs linking two adjacent spiral chains. These results demonstrate the advantage of polarized fluorescence XAFS as a means of non-destructive local probe of nanoscale structures and spatial modulations on solid surfaces.

1. Introduction

The advantage of X-ray absorption fine structure (XAFS) in a fluorescence mode is that one can probe the local structure with a high sensitivity (10^{19}/cm^3 or 10^{14}/cm^2) with a time scale of 10^{-15} sec. The use of insertion devices as high brilliance photon sources and dense-packed solid-state detector, the efficiency in fluorescence excitation and detection has greatly increased [1], making it possible to probe more dilute systems or dynamic aspects of electron states of solids. These features have been utilized in studies of nanoscale modulations in high T_c superconductors [2-4] or atomic rearrangements as a result of photoexcitation [5]. For $Bi_2Sr_2CaCu_2O_8$ [2] and $La_{2-x}Sr_xCuO_4$ [3], a two-dimensionally modulated "stripe" structure has been reported in the CuO_2 plane. For $YBa_2Cu_3O_{7-\delta}$, the local lattice anomalies were observed in the out-of-plane and in-plane Cu-O bonds [4]. For amorphous selenium (α-Se), It is found that inter-chain "dynamical" bonds are formed as a result of photoexcitation of lone pair electrons [5]. The results suggest that "photostructural change" in chalcogenide glasses is caused by a static disorder arising from photoinduced interchain bonds. In the following, we briefly describe the recent advances in fluorescence XAFS and report the results of *in-situ* XAFS studies of $YBa_2Cu_3O_{7-\delta}$ (temperature dependence) and α-Se (effect of photoexcitation).

2. Advances in Fluorescence XAFS

For applications of XAFS to nanostructures on solid surfaces, the use of a fluorescence detection technique is essential. For improving the efficiency of fluorescence detection, it is desired that both the brilliance of incident beam and efficiency of fluorescence detection are increased. For this purpose, a multipole wiggler (MPW) and a dense-packed solid state array detector were combined [1]. The calculated brilliance for the 27-pole wiggler magnet inserted to a 2.5 GeV storage ring at the Photon Factory is compared with that of a bending magnet in a logarithmic scale (top) and in a linear scale (bottom) in Fig. 1. The positions of absorption edges for various elements in a periodic table (Ca-Ce) are indicated. The calculated brilliance is greater than that of a bending magnet by a factor of 20-30 over a wide range in energy (4-30 keV) where K- and L- absorption edges for atoms with $Z > 20$ are distributed. The total power of MPW is 5.44kW for the magnetic fiele (B_0) of 1.5 T. The high heat load of MPW causes a serious problem which degrades the throughput and angular divergence of monochromatized X-ray beam. A directly water-cooled Si (111) monochromator is used which horizontally accepts ~4 mrad radiation.

Since the count rate of a solid state detector is limited by the dead time of electronics, a multi-element solid state detector is used for hiht efficiency fluorescence detection. The average

energy resolution for a 19-element Ge detector is ~180 eV at 5.9 keV [6]. Since each detector element can accept 1.5×10^5 cps with a reasonable energy resolution (~240 eV) using a 0.5 μsec shaping time, one can handle the total count rate of $\sim3\times10^6$ cps. Combining a detector array with an insertion device, the fluorescence detection efficiency increases by more than two orders of magnitude.

For a normal incidence geometry in a hard X-ray region, the penetration depth of incident beam and the escape depth of fluorescent X-rays are both much greater than a typical layer thickness of interest (several tens of angstrom). Using a grazing-incidence geometry and an energy discrimination of fluorescence spectra, surface sensitivity is dramatically improved. In a polarized fluorescence XAFS geometry shown in Fig. 2, vertical and horizontal sample orientations provide the information on radial distributions around an excited atom paralled and perpendicular to the surface normal, respectibely. In the following experiments, the electrical field vector is taken to be parallel to the surface.

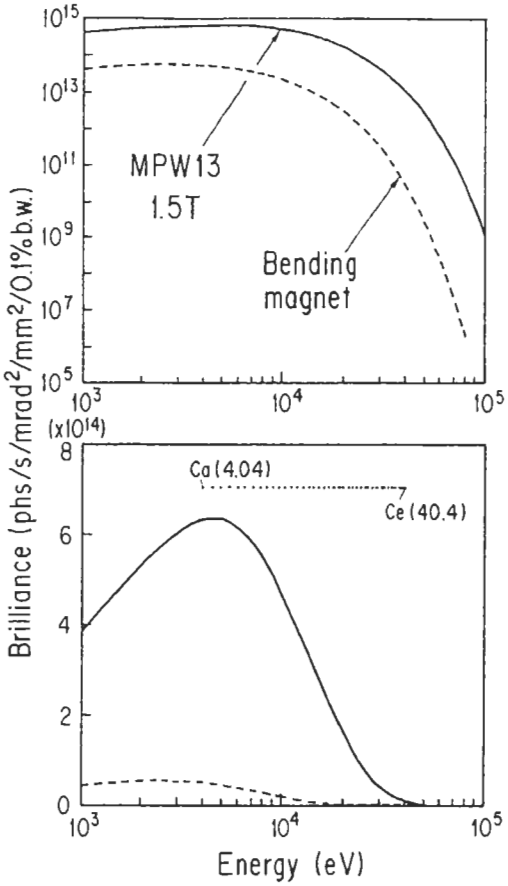

Fig. 1 Brilliance of a 27-pole wiggler magler magnet inserted to a 2.5 GeV storage ring at the Photon Factory, in comparison with that of a bending magnet in a logarithmic scale (top) and in a linear scale (bottom). The positions of absorption edges for elements with Z > 20 are indicated.

3. Lattice Anomalies in High T_c Superconductors

Figure 3 shows the temperature dependences of the mean-square relative displacements σ^2 for the Cu_1-O_4, the Cu_2-O_4 and the Cu_2-O_{eq} bonds in highly oriented $YBa_2Cu_3O_{7-\delta}$ thin film samples synthesized by a reactive coevapolation technique. The sample grown on the MgO substrate is about 1000Å thick and T_c value measured by a four-probe method is 87.5K. The anomalous increase of σ^2 observed at T_c is a general feature of the three kinds of Cu-O pairs. The temperature dependence of σ^2 is highly anisotropic; the out-of-plane Cu_2-O_4 and in-plane Cu_2-O_{eq} bonds show a large positive variation with T while the out-of-plane

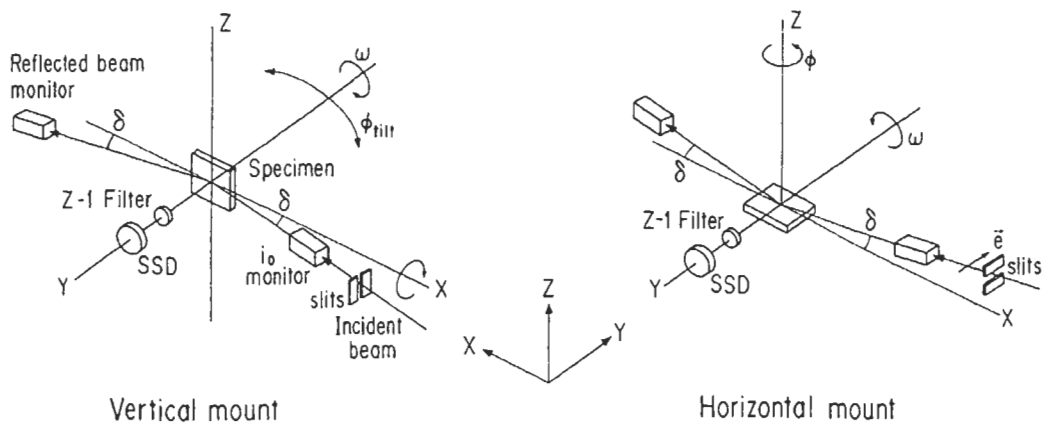

Fig. 2 Arrangement of a grazing-incidence fluorescence detection for the two polarization geometries. The sample is irradiated by monochromatized X-ray. Intensities of incident and reflected beams are monitored by and ionization chamber (i_0 monitor) and a secondary electron multiplier.

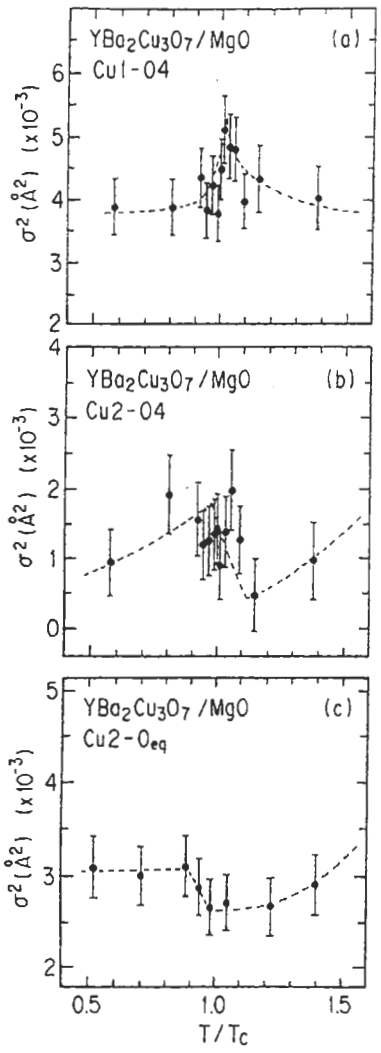

Fig. 3 Normalized temperature dependences of the mean square relative displacement in $YBa_2Cu_3O_{7-\delta}$ for (a) Cu_1-O_4, (b) Cu_2-O_4 adn (c) Cu_2-O_{eq} bonds.

Cu_1-O_4 bonds have much smaller temperature dependence. For the Cu_1-O_4 bond, σ^2 sharply increases at T_c while it is almost independent on T below $1.5T_c$. For the Cu_2-O_4 bond, σ^2 decreases with the decrease of T and sharply increases at T_c. These results indicate that the vibration of apical oxygen atom (O_4) increases at T_c. In contrast, σ^2 for the in-plane Cu-O_{eq} bonds deviates from a normal (positive) T-dependence below T^* ($\sim 1.5T_c$) as indicated by an arrow, which is followed by the sharp increase of σ^2 at T_c. This indicates that the Cu-O_{eq} vibration either hardens or has correlation occurs below T^*.

Summarizing the results, we find that the local lattice anomalies occur not only at T_c but also well above T_c. The mean-square relative

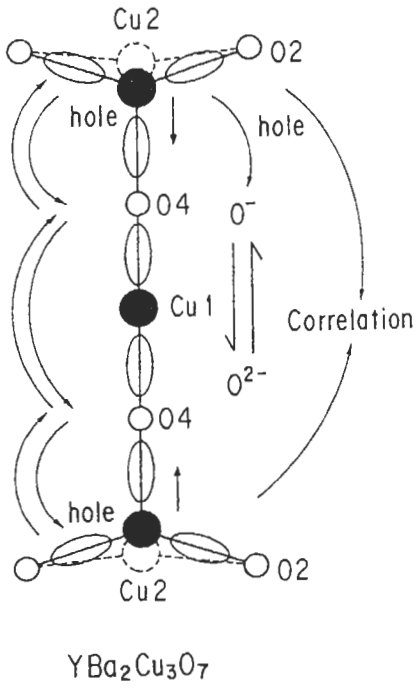

Fig. 4 Schematic local structure of $YBa_2Cu_3O_{7-\delta}$ along the c-axis. The in-plance Cu-O bond shows the anomaly belew $T^* \sim 1.5T_c$ while all Cu-O bonds show the anomaly at T_c.

displacements for the two out-of-plane Cu-O bonds (Cu_1-O_4, Cu_2-O_4) simultaneously increase at T_c. This indicates that the positions of apical oxygen atom (O_4) fluctuate around T_c. The in-plane Cu-O bonds show the anomalous decrease of relative displacement beginning at higher temperature than T_c. The observed in-plane lattice anomaly is consistent with anomalies in dynamical spin susceptibilities [7] or resistivity [8] which are interpreted in terms of spin-gap opening. These suggest that the in-plane anomaly below T^* is caused by the coupling between lattice (phonon) and magnetic excitations. The correlated displacement of apical oxygen atoms may induce a bilayer coupling associated with a charge transfer as illustrated in Fig. 4 The XAFS results strongly suggest the interplay between lattice effects and spin excitations. Within the framework of resonating valence bond (RVB) theory [9], the anomalies can be interpreted as the onset of short-range ordering of spin singlet.

4. Photostructural Change in Amorphous Selenium

In-situ XAFS experiments for α-Se under

illumination at low temperature (30K) show that the average coordination number of selenium atoms increases during the photoexcitation [5]. An increase of the average coordination number indicates that the three-fold coordinated sites are formed. The results evidence that the photoinduced defect states form the interchain Se-Se bond under illumination. Since these defect sites immediately relax to other metastable form after cessation of light, they have not been detected by previous *ex-situ* experiments. The formation of three-fold neutral defect-pairs give rise to a structural disorder as evidenced in the mean-square relative displacement which remains after the light cessation until the heat treatment recovers the initial state. The results suggest that the origin of photostructural change is the static disorder introduced when the inter-chain bonds are formed.

Figure 5 shows the variations of the normalized coordination number (top) and mean-square relative displacement (bottom) asscoiated with sequences of sample treatment, i.e., 1: as-prepared, 2: under illumination, 3: after illumination and 4: after annealing. The bond length is essentially independent on the photoexcitation except a slight substrate dependence due to the effect of strain. The coordination number increases reversibly in the sample kept under irradiation. Associated with the change in coordination, σ^2 also increases under light irradiation. After illumination, the change of coordination disappears while the light-induced structural disorder remains. Although the magnitude of structural disorder varies from sample to sample, the normalized change in both coordination number and σ^2 gave similar results. We conclude that this change of structure, averaged over all sites, indicates a locally increased coordination such as three-fold coordinated sites. Annealing of the irradiated sample at room temperature results in complete recovery of the initial values for both the coordination number and the disorder.

In Fig. 6, a schematic is shown to illustrate the photoexcitation of lone pair electrons and the formation of three-fold defect pairs. Photo-induced increase of the average coordination number (~4%) is transient: initial coordination is restored after switching off the light while the light-induced structural disorder remains. The present results are interpreted in the following: it is expected that the majority of photo-induced defect is three-fold coordinated neutral C_3^0 which are formed so that the two adjacent selenium atoms belonging to different chains are linked by an interchain bond. When one of the lone pair electrons are excited into conduction states and delocalized, the new bonding involving the other lone pair electrons would be formed. We expect that if the excitation occurs at two sites separated by a shorter distance than the intra-chain next nearest neighbor atom, these two sites are stabilized being linked by a new interchain bond.

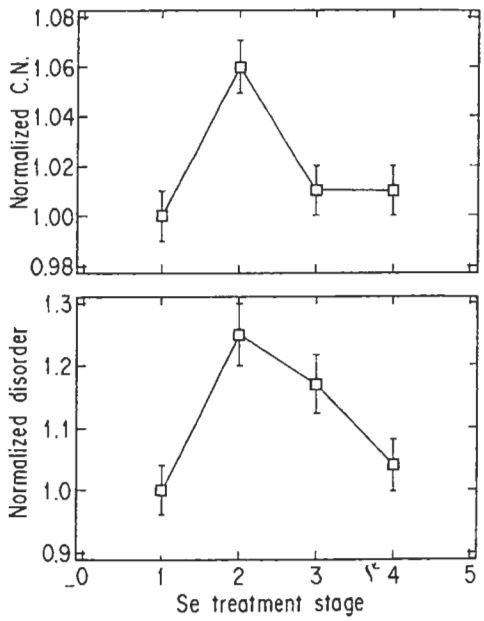

Fig. 5 The normalized coordination number (top) and the normalized mean-square relative displacement (bottom) plotted against the treatment stage (1: as-prepared, 2: under illumination, 3: after illumination and 4: after annealing at 300K).

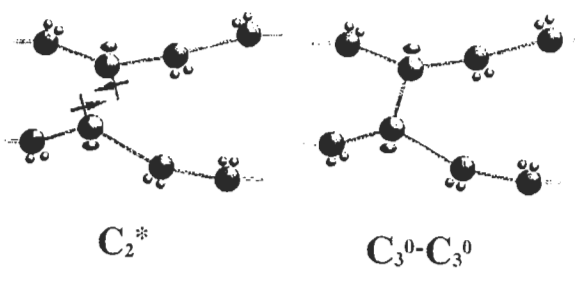

Fig. 6 A schematic diagram of the local structure and bonding in selenium chains as a result of illumination and after the illumination.

5. Conclusion

The advantage of XAFS as a "snapshot" local probe with a time scale of 10^{-15} sec is demonstrated by applications to high T_c suqerconductors. For $Bi_2Sr_2CaCu_2O_8$ and $La_{1.85}Sr_{0.15}CuO_4$, a two-dimensional modulated CuO_2 "stripe" structure has been observed. We find that in $YBa_2Cu_3O_{7-\delta}$, anomalies in the temperature dependence of mean-square relative displacement for the in-plance Cu-O bonds occur well above T_c. For amorphous selenium, it is fornd that the three-fold defect pairs are formed by photoexcitation. These results demonstrate capability of *in-situ* XAFS as a means of local probe for local and dynamical spatial modulations. In the future, the use of high brilliance photon sources such as X-ray undulator and FEL will allow us to analyze the time-resolved nanoscale structure.

References

1. H. Oyanagi, R. Shioda, Y. Kuwahara, K. Haga, J. Synchrotron Rad. 2 (1995) 99.
2. A. Binconi, M. Lusignoli, N.L. Saini, P. Bordet, A. Kvick and P.G. Radaelli, Phys. Rev. B54 (1996) 4310.
3. A. Bianconi, N.L. Saini, A. Lanzara, M. Missori, T. Rossetti, H. Oyanagi, H. Yamaguchi, K. Oka, T. Ito, Phys. Rev. Lett. 76, 3412 (1996).
4. H. Oyanagi, H. Kimura, T. Terashima, Y. Bando, J. Phys. Soc. Jpn. 64 (1995) 2563.
5. A. Kolobov, H. Oyanagi, Ka. Tanaka, Ke. Tanaka, Phys. Rev. B55 (1997) 726.
6. H. Oyanagi, M. Saito, M. Martini, to be published in Nucl. Instrum. and Methods.
7. M. Takigawa: A.P. Reyes, P.C. Hammel, J.D. Thompson, R.H. Heffner, Z. Fisk and K.C. Ott, Phys. Rev. B43 (1991) 247.
8. T. Ito, K. Takenaka and S. Uchida: Phys. Rev. Lett. 70 (1993) 3995.
9. P.W. Anderson, G. Baskaran, Z. Zou and T. Hsu: Phys. Rev. Lett. 58 (1987) 2790.